Supplement of Hydrol. Earth Syst. Sci., 29, 1505–1523, 2025
https://doi.org/10.5194/hess-29-1505-2025-supplement

Hydrology and Earth System Sciences
Open Access
EGU

Supplement of

Seasonal and diurnal freeze–thaw dynamics of a rock glacier and their impacts on mixing and solute transport

Cyprien Louis et al.

Correspondence to: Landon J. S. Halloran (landon.halloran@unine.ch) and Clément Roques (clement.roques@unine.ch)

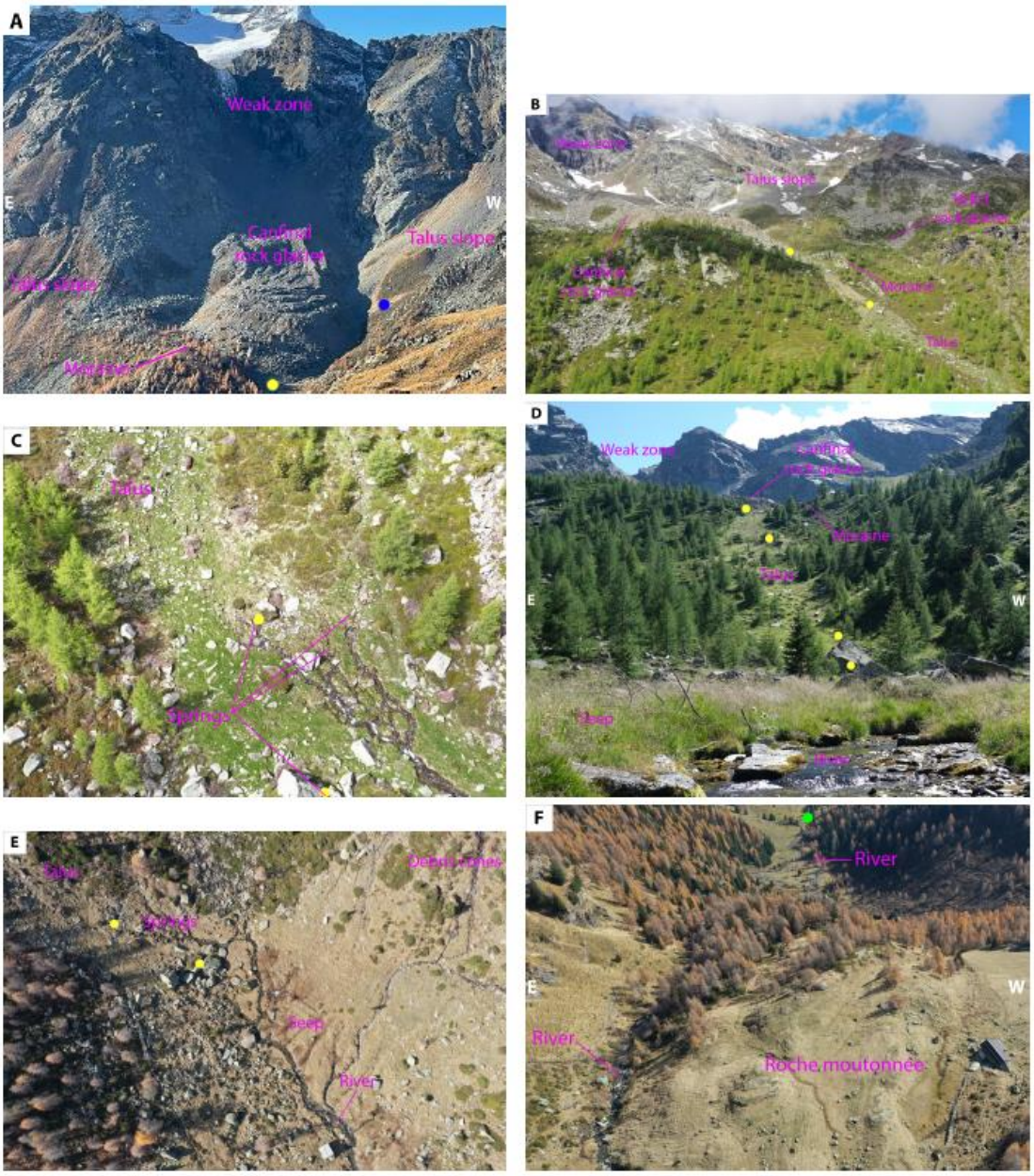

Figure S1: Illustrative view of some of the Quarternary features of the Val d'Ursé (UAV imagery and ground-level photography). The dots represent some of the monitored locations: the KB4 borehole (blue), the monitored springs (yellow) and the stream gauge (green). Monitored springs S1-S4 (numbered from highest to lowest) are all visible in D.

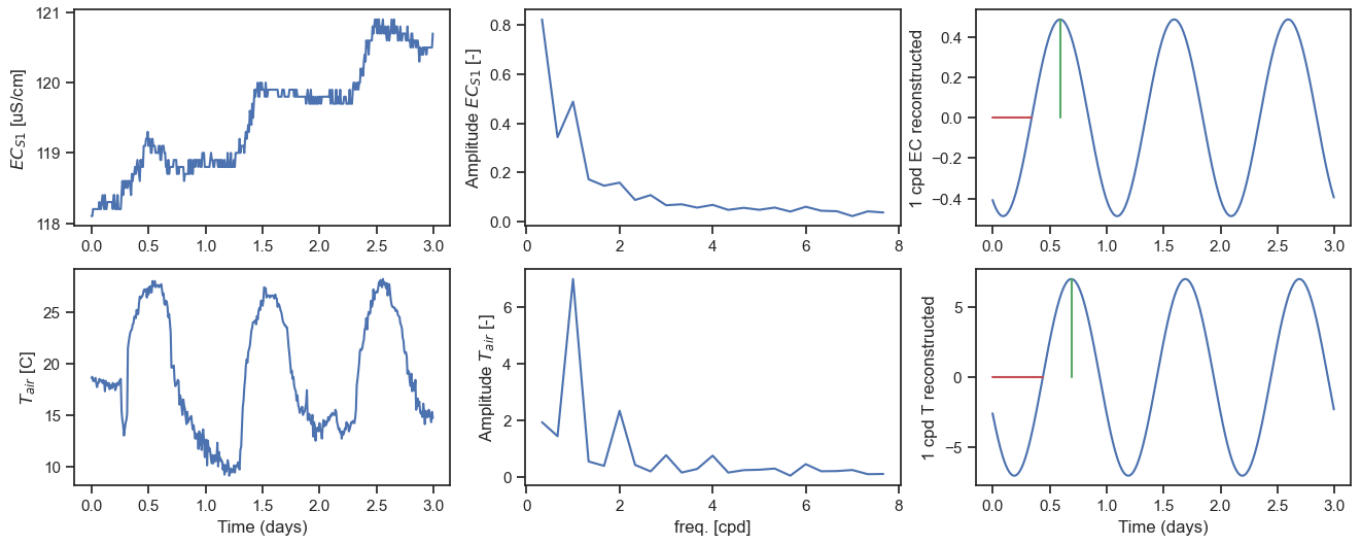

Figure S2: Illustration of an example 3-day window (i.e., corresponding to the window length in the frequency-domain analysis approach) of the EC (top) and air temperature (bottom) diurnal signal. Data is shown in both the time-domain (left) and frequency-domain (middle). The 1 cycle-per-day (cpd) components (right) are compared as part of our analyses. Here, we see how the 1 cpd component can be extracted from the rest of the data. The green lines indicate the amplitude and the red lines the phase for this particular window.

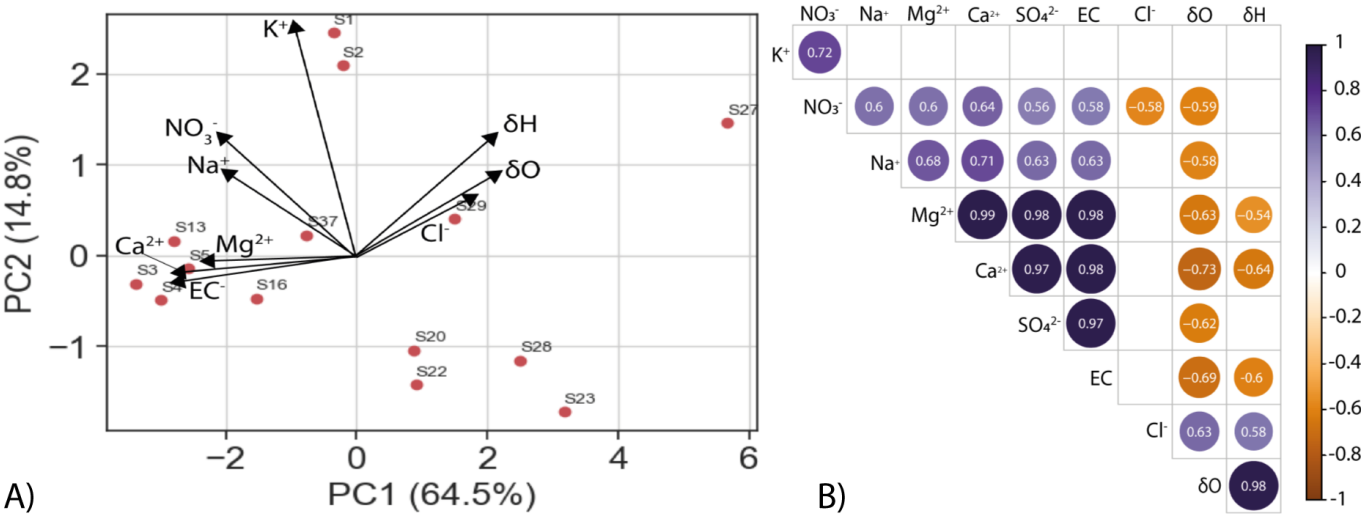

Figure S3: A) Principal component analysis (PCA) biplot of samples taken on 30.10.2022. B) Correlation matrix containing only the significant correlations between variables ($p < 0.05$). The color intensity and size of the circles are determined by the strength of the correlation (purple = positive correlation, gold = negative correlation). The number represents the correlation coefficient (r) for each correlation.

	Cl^-	NO_3^-	SO_4^{2-}	Na^+	K^+	Ca^{2+}	Mg^{2+}	δ^2H	$\delta^{18}O$	EC
S1	0.32	1.85	24.52	1.23	0.79	12.15	2.9	-68.31	-10.27	100.2
S2	0.16	1.64	22.94	1.31	0.71	11.75	2.76	-67.28	-10.15	96.2
S3	0.11	1.62	81.25	1.32	0.41	24.01	6.78	-70.94	-10.55	202
S4	0.13	1.35	79.2	1.3	0.41	23.43	6.63	-70.54	-10.53	199.5
S5	0.35	1.26	78.86	1.44	0.38	23.30	6.55	-69.93	-10.45	196
S13	0.32	1.32	77.58	1.42	0.46	23.55	6.60	-70.21	-10.49	197.8
S16	0.18	0.68	61.99	1.25	0.47	19.35	5.23	-70.18	-10.39	168
S20	0.38	0.84	15.46	1.11	0.32	10.19	1.65	-71.32	-10.55	74.6
S22	0.29	0.75	14.03	1.09	0.28	9.78	1.65	-71.71	-10.49	72.8
S23	0.4	0.23	5.28	0.7	0.16	5.54	1.23	-67.69	-9.94	85
S27	0.76	0.12	1.98	0.9	0.39	1.2	0.26	-60.52	-9.1	14.2
S28	0.18	0.72	5.76	0.87	0.21	4.81	1.28	-67.59	-10.03	41
S29	0.32	0.71	8.17	1.30	0.4	9.84	2.67	-66.69	-9.92	78.7
S37	0.49	0.93	36.67	1.67	0.43	14.37	3.57	-71.22	-10.51	119
PC1	0.25	-0.3	-0.36	-0.3	-0.14	-0.38	-0.37	0.29	0.33	-0.37
PC2	0.17	0.38	-0.04	0.28	0.73	-0.03	-0.01	0.38	0.26	-0.07

Table S1: Ion concentrations (mg/l), specific conductance (µS/cm) and stable isotopic values (‰ VSMOW) for the springs and streams sampled on 30.10.2022 in the Val d'Ursé, and variable loadings of these in the principal component analysis (PCA) (Figure S2).

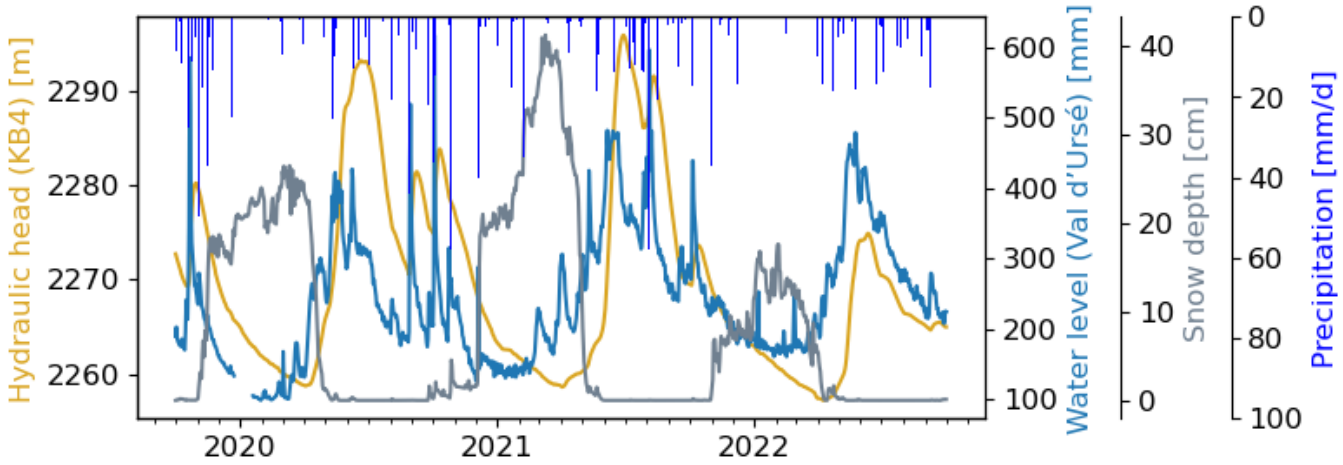

Figure S4: Time series of hydraulic head (KB4, orange), water level at Val d'Ursé stream (blue), snow depth (gray), and daily precipitation (blue bars) from 2020 to 2023. Hydraulic head and water level show seasonal variations primarily driven by snowmelt recharge, with additional evidence of efficient recharge during summer and fall storm events.